Chinese Chemical Letters 35 (2024) 109196

Contents lists available at ScienceDirect

Chinese Chemical Letters

journal homepage: www.elsevier.com/locate/cclet

Cocktail effect of ionic patch driven by triboelectric nanogenerator for diabetic wound healing

Yixia Zhang[a], Caili Xue[a], Yunpeng Zhang[a], Qi Zhang[a], Kai Zhang[a], Yulin Liu[a], Zhaohui Shan[b,c], Wu Qiu[e], Gang Chen[e], Na Li[e], Hulin Zhang[b,*], Jiang Zhao[d,*], Da-Peng Yang[e,f,*]

[a] College of Biomedical Engineering, Taiyuan University of Technology, Taiyuan 030024, China
[b] College of Electronic Information and Optical Engineering, Taiyuan University of Technology, Taiyuan 030024, China
[c] Shanxi-Zheda Institute of Advanced Materials and Chemical Engineering, Taiyuan 030024, China
[d] College of Integrated Circuit Science and Engineering, Nanjing University of Posts and Telecommunications, Nanjing 210023, China
[e] School of Rehabilitation Science and Engineering, University of Health and Rehabilitation Sciences, Qingdao 266024, China
[f] School of Materials and Chemical Engineering, Quanzhou Normal University, Quanzhou 362000, China

ARTICLE INFO

Article history:
Received 11 August 2023
Revised 8 October 2023
Accepted 9 October 2023
Available online 13 October 2023

Keywords:
iTENG
Cocktail effect
$CuFe_2O_4$
Eggshell
Diabetic wound

ABSTRACT

There is increasing evidence shows that either electrical stimulation (ES) or metal ion is an effective way to accelerate ulcerative wound healing. However, less attention is paid to investigating the synergistic effect between them. Herein, we explore the combined effects of ES and multiple metal ions on diabetic wound healing assisted by a triboelectric nanogenerator (TENG). Firstly, the novel Eggshell@$CuFe_2O_4$ nanocomposites (NCs) are prepared, which show unique structure and intrinsic antimicrobial properties. Subsequently, the as-prepared nanocomposites are embedded in oxidized starch hydrogel to form a multifunctional composite gel, which is further assembled into a wearable ionic triboelectric nanogenerator (iTENG) patch with polydimethylsiloxane (PDMS). It can convert the mechanical energy produced by a human body motion to electric energy and mediate the sequential release of metal ions (Fe^{2+}/Ca^{2+}/Cu^{2+}), thereby resulting in the "cocktail effect" on impaired tissue. Under their effects, a satisfying healing result in diabetic mouse is identified, which can effectively accelerate wound healing process by relieving inflammation, promoting angiogenesis and collagen deposition. The work puts forward the cocktail effect of electric simulation coupled with the multiple metal ions, and opens up a new perspective in designing iTENG patch towards repair of hard-to-heal wounds.

Chronic non-healing wound is one of the major threats to human health [1,2]. Especially, diabetic foot ulcers can cause the most serious threaten patients' life [3,4]. Therefore, it is highly urgent to find an effective way to promote tissue regeneration. In recent years, some metal ions (such as Ca^{2+}, Fe^{2+}, Cu^{2+}) have been used as therapeutic reagents to enhance tissue regeneration [5–7]. For example, Ca^{2+} is well known as an important factor in the wound healing process [8,9]. Fe^{2+} or Cu^{2+} as cofactors of some enzymes can facilitate collagen regeneration [10,11]. Particularly, the copper element is usually used as essential nutrient to stimulate angiogenesis [12,13]. Similarly, iron ions can enhance the secretion of vascular endothelial growth factor (VEGF), angiopoietin-1 and fibroblast growth factor-2 (FGF2), which contribute to the proliferation and migration of endothelial cells, and increase the re-epithelialization on wound tissue [14,15]. Although each kind of metal ion has been studied for certain biological function, there are few reports regarding the synergistic physiological capability of combined metal ions on wound tissue regeneration. Since the ions concentration has not been accurately and quantitatively controlled, metal ions-based treatment is largely hindered. Therefore, a controllable ions platform with penetration depth and transmembrane transport efficiency is urgently anticipated to explore metal ions-based wounds healing. Meanwhile, ions movement across cell membrane can generate electrical signals through tissue spaces, which play an important role for cell-to-cell communication. When the integrity of the skin is damaged, an endogenous electric field will be generated in the wound and a series of physiological reactions will be initiated to close the wound [16,17]. The natural endogenous electrical potentials around a wound are known to accelerate the healing process

* Corresponding authors.
E-mail addresses: zhanghulin@tyut.edu.cn (H. Zhang), jzhao@njupt.edu.cn (J. Zhao), yangdp@qztc.edu.cn (D.-P. Yang).

https://doi.org/10.1016/j.cclet.2023.109196
1001-8417/

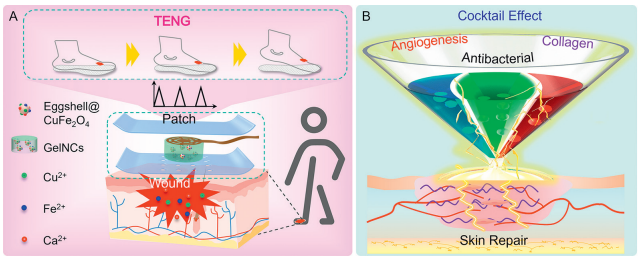

Fig. 1. (A) Schematic illustration of the structural design features and working mechanism for the ionic patch driven by TENG. (B) The cocktail effects between TENG and GelNCs induce collagen deposition, angiogenesis as well as antibacterial for diabetic wound.

by guiding cells to migrate to injury site [18,19]. Recently, triboelectric nanogenerator (TENG) producing self-sustainable electrical stimulation also shows great potential in wound management [20–22]. Considering the importance of both metal ions (such as Fe^{2+}, Cu^{2+}, Ca^{2+}) and TENG in accelerating wound healing, it is worth developing a kind of related nanocomposites triggered by TNEG to relieve active ions and repair skin wounds. Herein, the unique structure Eggshell@$CuFe_2O_4$ nanocomposites (NCs) were prepared. And antimicrobial activities were investigated by bacteria and fungi. Then, they were entrapped into starch gel to prepare ions-trapped hydrogel. The periodic electrical field generated by TENG can control the quantitative release of metal ions from the gel, which was accumulated on wound part to display cocktail effect. Pig skin model was used to investigate the transepithelial delivery efficiency of metal ions from gel under electrical stimulation. A full-thickness skin defect diabetes mice model was used to evaluate the synergistic effects.

Since metal ions and electrical potential simulation play important roles during the process of wound repair, a functional patch is designed. The components and biological activities of ionic patch driven by TENG are schematically illustrated. In Fig. 1A, the patch is made up of two-layer polydimethylsiloxane (PDMS) membranes, the Eggshell@$CuFe_2O_4$ nanocomposites hydrogel (GelNCs) conductive hydrogel are sandwiched in between them (Fig. S1 in Supporting information). It is worth noting that some holes with a 4×4 array are chiseled on one side of PDMS membrane to fit the GelNCs. The patch with porous PDMS side is attached to the wound surface. TENG can effectively reduce inflammation and speed up the cell proliferation [23]. Meanwhile, TENG can also quantitatively impel mental ions release from GelNCs to wounds. Additionally, the current-voltage (*I-V*) curves of GelNCs samples with different concentration of NCs and compression stress−strain curves were also shown in Fig. S2 (Supporting information). The organized periodic metal ions release is vital to activate the corresponding biochemical pathways in a timely manner. We are hopeful that these metal ions accumulated on wound will display the advantages of antimicrobial effect, collagen deposition and angiogenesis under the influence of electrical simulation (Fig. 1B), which come into operating cocktail effect to accelerate wound healing.

The typical preparation route of the GelNCs is displayed in Fig. 2A. First, the fine powder was mixed with $CuCl_2$ and $FeCl_3$ to form a homogeneous solution, which was transferred into a stainless-steel vessel to synthesize Eggshell@$CuFe_2O_4$ (NCs). Subsequently, a certain amount of NCs was added into starch gel to obtain the GelNCs. Last, the GelNCs was sandwiched between two layers of PDMS membranes to form a patch. The GelNCs-based patch was attached to the wound to schematically outline the working principle driven by TENG (Fig. 2B). The metal ions motion with different electrical field intensities was simulated by COMSAL. A group of representative photographs were captured (Fig. 2C), which indicated the moving pathways of metal ions exposed to the different electric fields. A video was shown in Supporting information. This simulation results showed that an appropriate electric field could drive metal ions to move towards a certain direction and distance. However, metal ions will undergo disordered motion with limited distance without external electrical field.

To reveal the surface characteristics of the GelNCs, scanning electron microscope (SEM) images at different magnifications were recorded. As shown in Fig. 2D, some porous structures with pores ranging from 20 μm to 50 μm could be seen on the flat surface of the GelNCs. Furthermore, a high-magnification image clearly shows the micro-structure of the pores. As shown in Fig. 2E, some humps can be found in the walls of holes in-depth, which belong to the NCs. Moreover, electrical field intensity distribution was simulated by COMSOL (Fig. 2F). In the pores, the electrical field is positive and much smaller than the outside parts of pores. This will facilitate ions movement across the pores. In addition, energy dispersive spectrometer (EDS) elemental mapping images further illustrate the elemental composition and distribution of the nanocomposites. As shown in Figs. 2G–I, the elements of Cu, Fe, Ca homogeneously distributed in the GelNCs. In addition, the total elements mapping, Fourier transform infrared (FTIR), as well as X-ray diffraction (XRD) pattern were shown in Fig. S3 (Supporting information).

The antimicrobial activities were firstly evaluated against both bacteria and fungus. Fig. 3A showed the photographs of the colony numbers based on different concentrations of Eggshell@$CuFe_2O_4$ NCs, which indicated that the antimicrobial capability increased in a dose-dependent manner. Obviously, the Eggshell@$CuFe_2O_4$ NCs displayed excellent antimicrobial activity even with a relatively lower concentration (10 mg/mL). The antibacterial rates with 10 mg/mL NCs were 84.94%, 79.86%, 82.88% and 90.14%, against *Escherichia coli* (*E. coli*), *Staphylococcus aureus* (*S. au*), *Pseudomonas aeruginosa* (*P. ae*), *Saccharomyces cerevisiae* (*S. ce*), respectively (Fig. 3B). Moreover, the bacteriostatic rates of *E. coli*, *S. au*, *P. ae* and *S. ce* reached up to 94.07%, 93.77%, 97.04% and 93.63% at the concentration of 20 mg/mL. No colonies were found with 30 mg/mL of NCs for all microbes. These data indicate that NCs have broad-spectrum antimicrobial activities on both bacteria and fungi. The robust antimicrobial activities mainly originate from the release of metal ions, which damage the integrity of microorganisms [24–26]. It could be identified by a series of gradients color change following the increasing concentrations of Eggshell@$CuFe_2O_4$ NCs in suspension (Fig. 3C). As shown in Fig. S4A (Supporting information) the higher the concentration of NCs, the larger and the darker color of the antibacterial zone, indicating that there are more ions-releasing from ES@$CuFe_2O_4$. Fig. S4B (Supporting information) is the representative photo of Eggshell@$CuFe_2O_4$ in phosphate buffer saline (PBS) solution keeping for different time (0–24 h). It is clear that a significant gradient change occurs in the color of the Eggshell@$CuFe_2O_4$ PBS solution, which indicates that ions continue to release over time.

In addition, the antimicrobial ability of both NCs and GelNCs was done. As shown in Figs. 3D–G, the diameter of inhibition zone (DIZ) of NCs for *E. coli*, *S. au*, *P. ae* and *S. ae* were 11.8, 14.03, 11.03 and 24.5 mm, respectively. In contrast, the DIZ of GelNCs was relatively smaller. The reduced antimicrobial activity can be attributed to the restricting effect of starch gel, which delays the release of metal ions. Moreover, ultraviolet–visible spectroscopy (UV–vis) curves in Fig. S5 (Supporting information) also indicated the restricting effect of starch gel for NCs. Hence, the wearable patch will display customizable metal ions release and antimicrobial abilities under TENG control. Additionally, there is clearly visible brown color on the gauze under the pigskin with the TENG treatment. Which suggested that the TENG can promote ions release and drive ions transport over pigskin tissue (Figs. S4C and S6 in Supporting information). As a control group, no color change was observed without TENG.

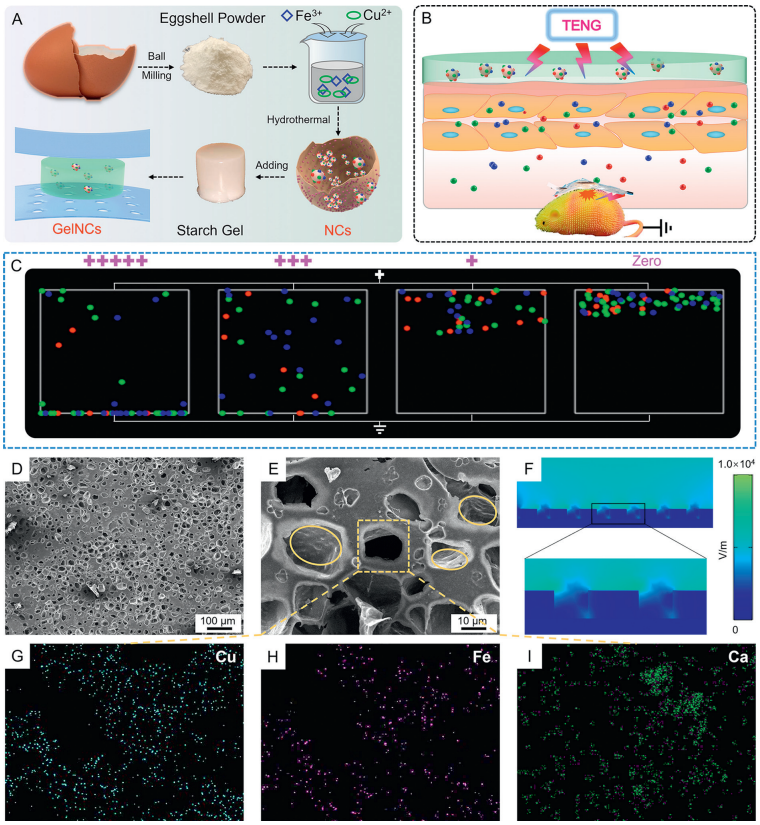

Fig. 2. (A) Schematic diagram of the fabrication of GelNCs. (B) Working model of patch attached to the mouse wound. (C) Simulation of the ions movement with different potential values by COMSOL. (D) Low-magnification and (E) high-magnification of images of GelNCs. (F) Electrical field intensity distribution simulated by COMSOL. (G–I) The concerned elemental mapping in GelNCs.

The working principle of TENG driven ionic patch is based on the coupling effect of contact electrification and electrostatic induction, which can be traced back to the Maxwell equations [27]. Here, the mechanism of TENG during walking was schematically described (Fig. 4A). In the beginning, the leather layer and PDMS layer carry equal charges with opposite polarity at contacted stage. While walking, the leather layer will separate from the PDMS layer, the balance will be broken. Since the PDMS layer will induce ionic movement. Thus, some positive charges will be produced on the surface of GelNCs and their amount will depend on the separating distance. When the gap is further widened, more positive charges will be generated on the surface of GelNCs. Contrarily, when the gap becomes narrow, the positive charges will become less and less until electrical equilibrium. The vertical contact–separation mode dominates the electric field as TENG, which enhances keratinocyte–fibroblast proliferation and thus accelerates wound healing [23,28]. Besides, the TENG field can regulate metal ions release rate and penetration depth from the conducting GelNCs, which was conducive to display the cocktail effect. Further, the simulated electric potential distribution is displayed in Fig. 4B. When the separation distance increases, the hydrogel always carries the positive charges, which will drive the positively charged ions to the impaired skin and guide ions movement. To further test the devices' bendable performances, electrical output of the device with different angles was determined. As shown in Fig. 4C (left), it is found that the output voltage has tended to reduce with the increase of bending angles. However, it keeps a stable electrical output at the same angle with different time, which indicated that the TENG patch can work well. Moreover, the influence of different Eggshell@$CuFe_2O_4$ NCs concentrations on the output voltage of TENG patch is also analyzed. As shown in Fig. 4C (right), the average output voltage value of TENG patch without nanocomposites is a little smaller than that of adding different concentrations Eggshell@$CuFe_2O_4$ NCs, and the curves of the output voltage for different nanocomposites concentrations almost keep rather stable with different time, which imply that the nanocomposites concentrations do not significantly influence the performance of the device. In clinics, patients with diabetic foot often undergo intermittent claudication due to ulcers, pain, *etc.* So, the output voltage will be reduced along the decrease of contact area between foot and TENG patch when walking. Therefore, it is necessary to simulate the output of open circuit voltage with different degrees of intermittent claudication. As shown in V-time curve (Fig. 4D), curve I simulates the voltage output during the walking process of early diabetic foot patients. In about 4 s, the output voltage of the TENG patch ranges from 44.87 mV to 67.19 mV, with an average value about 54.11 mV. Further simulation of the symptoms of diabetic foot patients aggravated to a certain extent is shown in curve II. Compared with curve I, only 4 pulse voltages are generated within 4 s due to the slower walking speed of the patient. It takes about 6 s to generate voltage of the same frequency (6 pulses), and the period time is extended. And, the voltage of the TENG patch ranges from 53.59 mV to 69.51 mV, with an average value about 60.87 mV. As shown in curve III, when the symptoms of diabetic foot are further aggravated, the walking speed of patients is further decreased, and the duration of a single pulse is prolonged in curve III. And the foot contact area was greatly decreased due to the aggravation of ulcer pain. Within 6 s, the voltage of TENG patch is only about 30 mV. Compared with curve II, the voltage of TENG patch in curve III decreases by half. The above data show that the TENG patch has a certain level of voltage generation, which can drive therapeutic ions to promote wound healing.

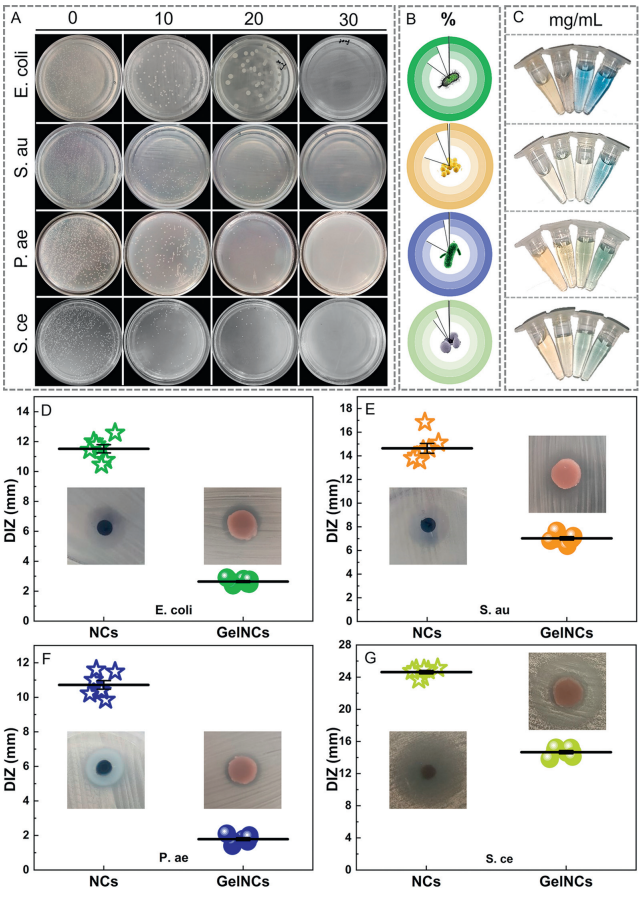

Fig. 3. Antimicrobial activities of Eggshell@$CuFe_2O_4$ NCs and GelNCs against *E. coli*, *S. au*, *P. ae* and *S. ce*. (A) The colony numbers with different concentrations of NCs (0, 10, 20, 30 mg/mL). (B) Antimicrobial rates for different concentrations Eggshell@$CuFe_2O_4$ NCs. (C) Pictures of different concentrations of Eggshell@$CuFe_2O_4$ NCs solution (0–30 mg/mL). (D–G) Comparisons of the DIZ between Eggshell@$CuFe_2O_4$ NCs and GelNCs ($n = 6$). All experimental results were expressed as a mean ± standard deviation (SD).

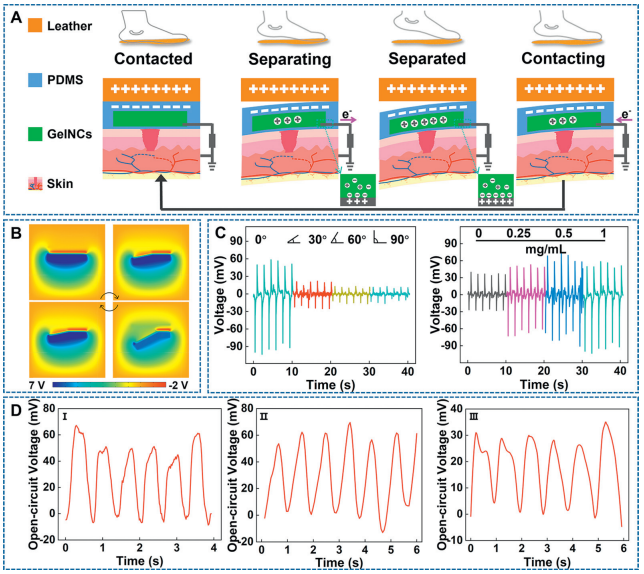

Fig. 4. Working mechanism and output performance of iTENG patch. (A) The diagram of working schematic at different walking stages. (B) Diagram of the electric potential distribution simulated with COMSOL. (C) Curves of output voltage: the left graph for different walking stage and the right graph for different concentrations of Eggshell@$CuFe_2O_4$ addition. (D) The open-circuit voltage of the TENG device applied to simulate different walking states.

To further evaluate the TENG can promote metal ions release from the GelNCs and transdermal transport rate, the porcine skin and treated eggshell as models were carried out (Fig. S6 in Supporting information). The results indicated that metal ions could be effectively released from the GelNCs and transported over the porcine skin tissue and porous eggshell within a certain electric stimulation period. As a comparison, the metal ions alone cannot penetrate over the porcine skin model without electric stimulation in the same time, revealing that the TENG-induced electrical stimulation is efficient for controlling the metal ions penetration depth over skin tissue.

Besides, to identify the biocompatibility of GelNCs and NCs, The HDF cells viability with different concentrations of NCs was carried out by MTT assay. The result showed that the viability of HDF cells remained about 85% (Fig. S7 in Supporting information) when the concentration of solution was generally 2 mg/mL or less (0.25, 0.5 and 1 mg/mL). The blood compatibility of different concentrations of GelNCs (0, 0.25, 0.5, 1 and 2 mg/mL) was also carried out. And the hemolysis activity of GelNCs was tested by direct contacting method. The supernatant was almost colorless as the red blood cells (RBCs) were sedimented at the bottom. As shown in Fig. S8A (Supporting information), the hemolysis percentage of all GelNCs groups were at 0.4%–1.6%, which were rather lower compared to the maximum limit (5%), indicating that GelNCs behave excellent blood compatibility. Furthermore, the HDF cell exhibited good morphology and integrity of cell membrane cultured with 1 mg/mL NCs over 48 h (Fig. S8B in Supporting information). And the biocompatibility of GelNCs extracts (1-$GelNCs_1$; 2-$GelNCs_2$; 3-$GelNCs_3$; 4-$GelNCs_4$) for HDF cell was investigated after incubation for 1, 3 and 5 days respectively. These results are illustrated in Fig. S8C (Supporting information). The HDF cell exhibited higher proliferation in all GelNCs extracts due to releasing essential active ions (*e.g.*, Ca^{2+}, Fe^{2+}, Cu^{2+}) as supply for cells. Thus, the GelNCs and NCs were considered to be good cytocompatibility.

To investigate synergistic effects of the TENG generated electrical pulse (EP) stimulation and multifunctional GelNCs, *in vivo* experiments were conducted by diabetic wound model. The mice experimental were approved by the Ethics Committee of Taiyuan University of Technology. An 8 mm round full-thickness skin wound was created on the back of diabetic mice and the mice were randomly divided into four groups. One group without any treatment was marked as the control group (Con). The other three groups were treated with NCs, EP, or NCs + EP, respectively. Additionally, the body weight and blood glucose of all groups were recorded (Fig. S9 in Supporting information). Representative photographs of wounds were collected on 0, 3, 7, 11, 14 and 21 days with different treatments, as shown in Fig. 5A.

Compared with control group, the wound area of all experimental groups showed significant wound closure, revealing the positive healing effect. Furthermore, the healing rates of wounds were charted in Fig. 5B. As anticipated, NCs + EP group demonstrated the fastest healing degree than other groups. Moreover, the epithelialization in the NCs + EP group was almost completely formed and hairs regeneration could be observed (Fig. 5A), compared to the control and single treatment, in which the wounds had not been completely healed. Furthermore, quantitative comparison of healing rate on the 3rd day was charted in Fig. 5C. Clearly, the healing rate was only 27.11% ± 5.39% for the Con group. While the repaired wound degree has been significantly improved regardless of NCs (38.76% ± 3.76%) or EP (44.56% ± 8.08%) treatment. It is worth noting that the wound healing rate was most effective and reached at 56.66% ± 8.20% with NCs + EP treatment. Moreover, the wound healing rate of the NCs + EP group was up to 86.34% ± 2.48% on the 7th day, which is much better than that of the NCs (53.41% ± 7.73%) or EP (57.9% ± 4.27%) group (Fig. 5D). As a result, the

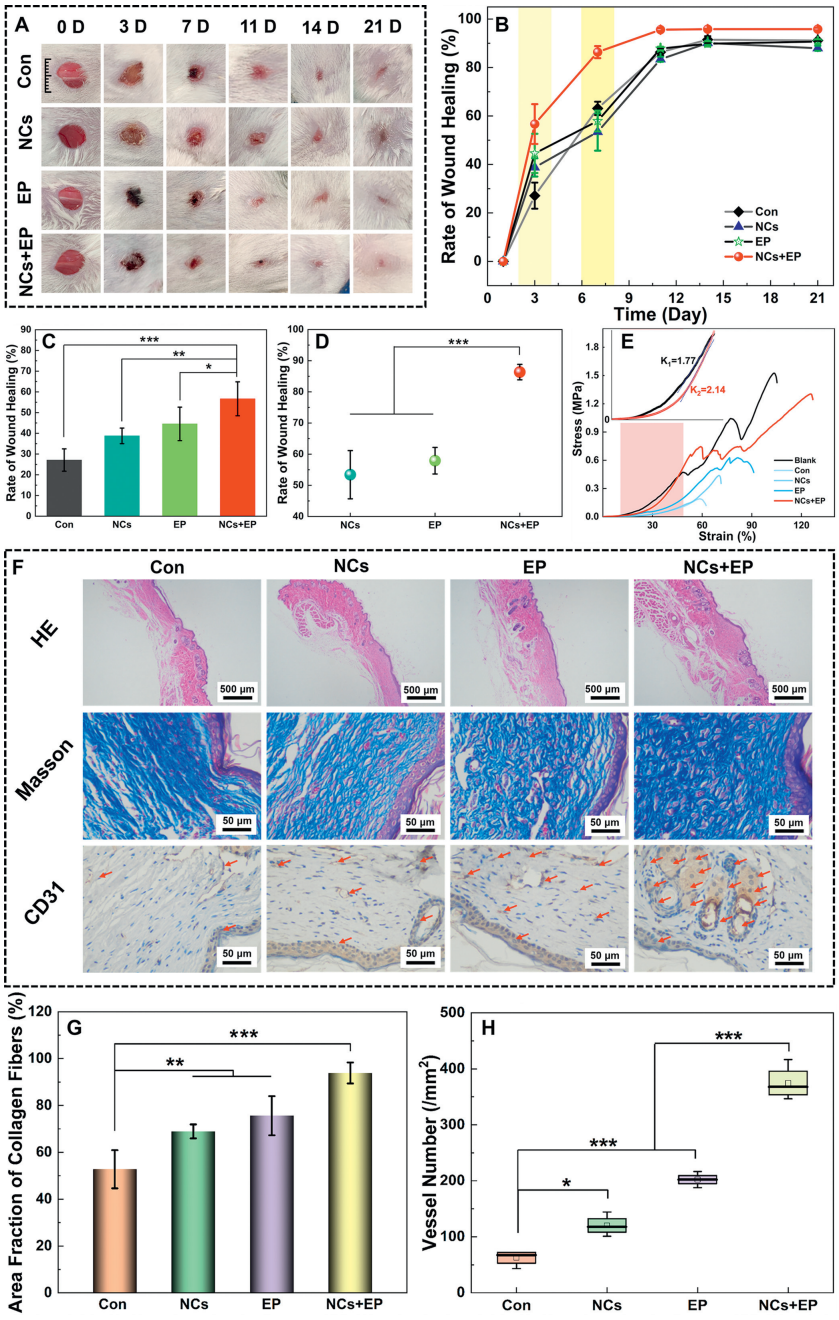

Fig. 5. (A) Representative photos of skin wounds with different treatments on 0, 3, 7, 11, 14, and 21 days, respectively. Scale bar: 10 mm. (B) Curves of wound healing rate at different time ($n = 6$). Statistical analysis of healing rate (C) on the 3rd day and (D) on the 7th day ($n = 6$). (E) Curves of the stress-strain of wound skin samples. The insert is the linear region of 0–45% strain. (F) H&E, Masson's trichrome and CD31 immunohistochemistry staining. Red arrows indicate the blood vessels. (G) Chart of quantitative statistics of collagen fiber of Masson's trichrome and (H) density of blood capillary CD31 staining. All experimental results were expressed as a mean ± SD. $^{*}P < 0.05$, $^{**}P < 0.01$, $^{***}P < 0.001$.

combined therapy by electric field and metal elements exhibited remarkable efficacy to promote wound repair.

Mechanical tensile test and elongation rate are critical for evaluating the skin tissue. The stress-strain curves of wound skin samples were described in Fig. 5E. Notably, the highest tensile strength (1.3 MPa) was obtained with NCs + EP treatment. Particularly, the mechanical strength of NCs + EP group was substantially improved more than 6.8 times compared with Con group. More importantly, the tensile strength of NCs + EP group was almost close to 1.52 MPa of the blank group skin sample (healthy mice). Additionally, the elongation rate of NCs + EP group reach up to 126.98%, which is significantly higher than other groups' elongation rates of 63.01%, 71.66%, 92.47%. It indicated that there is enough amount collagen in NCs + EP skin tissue, which was mainly attributed to the "cocktail effects" of the combination of EP and NCs treatments. Generally, there is a linear stage over the strain-stress curve, which demonstrated the elasticity of skin tissue. Similarly, a good linear stage at 30%–45% strain over the strain-stress curve of skin tissue from NCs + EP group, as described the insert in Fig. 5E. Generally, the linear fitting correlative coefficients ($k_2 = 2.14$) stands for the Young's modulus of the skin tissue. Notably, the k_2 was slightly bigger than that of the blank group ($k_1 = 1.77$). These results revealed that the elasticity of skin tissue with NCs + EP treatment was similar to that of healthy skin. These characteristics are mainly attributed to the larger amount of deposition and oriented arrangement of collagen molecules and filaments [29]. Obviously,

the synergistic effects interplayed and coordinated both EP and several metal ions, which can significantly accelerate more collagen synthesis, deposition and organization.

The process of wound healing mainly included granulation formation, collagen deposition and re-epithelialization [30]. The higher degree of collagen deposition and the better proliferated granulation tissues induce the faster wounds healing efficiency [31,32]. Hematoxylin-eosin (H&E) staining, Masson's trichrome and CD31 immunohistochemistry were performed to evaluate the wound healing mechanism (Fig. 5F). The NCs + EP group was almost epithelized and almost invisible inflammatory cells. Additionally, a large number of hair follicles and almost intact skin structure were observed in NCs + EP group. However, the physiological structure of the control group was still incomplete and even hypertrophied. This confirms that the NCs + EP treatment is more effective to reconstruct impaired skin.

The collagen deposition in a sufficient and orderly manner is a critical process in wound healing [33,34]. Masson's trichrome staining revealed the presence of well-organized and thicker collagen deposition on the wound bed after treatment with NCs + EP, which was similar to that observed in normal skin (Fig. 5F). The quantification of Masson's trichrome demonstrates that the area fraction of collagen fibers in the Con, NCs, EP, and NCs + EP groups is 52.76% ± 8.15%, 68.92% ± 2.99%, 75.61% ± 8.34%, and 93.87% ± 4.48%, respectively (Fig. 5G). It is evident that the NCs + EP treatment results in significantly greater collagen content compared to the NCs ($P < 0.001$), or EP treatment alone ($P < 0.01$).

Angiogenesis plays a crucial role in wound healing, and endothelial cell adhesion molecule-1 (CD31) is a key marker for angiogenesis assessment [35]. CD31 staining in Fig. 5G revealed a substantially higher number of CD31-positive cells in the NCs + EP group, while other groups exhibited relatively fewer capillaries. The capillary densities were 62.56 ± 16.67, 120.31 ± 22.05, 202.12 ± 14.44, and 374.71 ± 37.06 microvessels/mm^2 for the Con, NCs, EP and NCs + EP groups, respectively (Fig. 5H). This demonstrated a significantly greater degree of angiogenesis in the NCs + EP group than the other groups ($P < 0.001$). Notably, NCs and EP groups also displayed a marked increase in capillary density in comparison with Con group. Overall, the TENG also can regulate the periodic quantitative release of metal ions from GelNCs together with electric stimulation to display "cocktail effect" for enhance tissue regeneration.

In summary, in order to synthesize a multi-metal component nanocomposite, eggshell was used as bio-template to obtain the Eggshell@$CuFe_2O_4$ NCs. Based on starch hydrogel embedded Eggshell@$CuFe_2O_4$ and TENG, a flexible and wearable ionic TENG patch was developed for accelerating diabetic wound healing. The metal ions release from nanocomposites can be regulated by TENG to exhibit the cocktail effect. Furthermore, the nanocomposite contains Ca/Cu/Fe elements supply nutrient for cell. The TENG patch was systematically investigated for anti-inflammatory, angiogenesis and collagen deposition upon on diabetic animal wound. The TENG device will provide a new approach to efficiently regulate metal ions release and deliver them to transmembrane transport, which can be useful as a novel dressing for the treatment of chronic non-healing wounds.

Declaration of competing interest

The authors declare that they have no known competing financial interests or personal relationships that could have appeared to influence the work reported in this paper.

Acknowledgments

This work was supported financially by the Natural Science Foundation of Shanxi Province Grants (No. 202203021211157). Shanxi-Zheda Institute of Advanced Materials and Chemical Engineering (No. 2023SX-FR006). The Science and Technology Major Special Plan Project "Reveal the Tile" of Quanzhou Province (No. 2022NZ1).

Supplementary materials

Supplementary material associated with this article can be found, in the online version, at doi:10.1016/j.cclet.2023.109196.

References

[1] G. Han, R. Ceilley, Adv. Ther. 34 (2017) 599–610.
[2] S. Cheng, M. Pan, D.R. Hu, et al., Chin. Chem. Lett. 34 (2023) 108276.
[3] G.T. Liu, Y. Zhou, Z.J. Xu, et al., Chin. Chem. Lett. 34 (2023) 107705.
[4] P.K. Xin, S.Y. Han, J. Huang, et al., Chin. Chem. Lett. 34 (2023) 108125.
[5] J. Zhang, L. Chen, J. Wang, et al., Adv. Funct. Mater. 33 (2022) 2211237.
[6] M.A. Rahman, M.S. Islam, P. Haque, et al., Materialia 13 (2020) 100839.
[7] W. Ma, X. Zhang, Y. Liu, et al., Adv. Sci. 9 (2022) 2103317.
[8] L. Hudson, M. Begg, B. Wright, et al., J. Cell. Physiol. 236 (2021) 8171–8183.
[9] T. Subramaniam, T. Subramaniam, Y. Lokanathan, J.X. Law, Int. J. Mol. Sci. 22 (2021) 6486.
[10] B.R. Rao, R. Kotcherlakota, S.K. Nethi, ACS Biomater. Sci. Eng. 4 (2018) 3434–3449.
[11] X. Qi, J. Gan, Z. Zhao, et al., Langmuir 39 (2023) 2631–2640.
[12] J. Xiao, S. Chen, J. Yi, H. Zhang, G.A. Ameer, Adv. Funct. Mater. 27 (2017) 1604872.
[13] D. Li, J. Li, S. Wang, Q. Wang, W. Teng, Adv. Healthc. Mater. 12 (2023) 2203063.
[14] J. Xiao, Y. Zhou, M. Ye, Adv. Healthc. Mater. 10 (2021) 2001591.
[15] V. Coger, N. Million, C. Rehbock, et al., Boil. Trace Elem. Res. 191 (2019) 167–176.
[16] R. Luo, Y. Liang, J. Yang, et al., Adv. Mater. 35 (2023) 2208395.
[17] M. Zhao, B. Song, J. Pu, et al., Nature 442 (2006) 457–460.
[18] Y. Chen, L. Ye, L. Guan, et al., Biol. Open 7 (2018) bio035204.
[19] S. Shaner, A. Savelyeva, A. Kvartuh, Lab Chip 23 (2023) 1531–1546.
[20] D. Wan, J. Yang, X.J. Cui, Nano Energy 89 (2021) 106465.
[21] S.H. Bhang, W.S. Jang, J. Han, et al., Adv. Funct. Mater. 27 (2017) 1603497.
[22] W. Wang, W. Sun, Y. Du, et al., ACS Nano 17 (2023) 9793–9825.
[23] W. Hu, X. Wei, L. Zhu, Nano Energy 57 (2019) 600–607.
[24] L. Hu, Y.X. Wang, Q. Liu, et al., Chin. Chem. Lett. 34 (2023) 108262.
[25] Y.X. Wang, C.X. Zhang, H. Zhang, L.H. Feng, L.B. Liu, Chin. Chem. Lett. 33 (2022) 4605–4609.
[26] Y.C. Jin, S.X.C. Chen, P.W. Huang, et al., Chin. Chem. Lett. 34 (2023) 108444.
[27] X.A. Shen, W.J. Han, Y.F. Jiang, et al., Energy Rep. 6 (2020) 2851–2860.
[28] T. Sato, T. Lee, F. Takamatsu, T. Fujikado, Neuroreport 19 (2008) 1617–1621.
[29] D. Haluszka, J. Harsfalvi, M.S. Kellermayer, Biophys. J. 118 (2020) 40a–41a.
[30] D.R. Griffin, W.M. Weaver, P.O. Scumpia, D.Di Carlo, T. Segura, Nat. Mater. 14 (2015) 737–744.
[31] G. Chen, Y. Yu, X. Wu, et al., Adv. Funct. Mater. 28 (2018) 1801386.
[32] H. Chen, Y. Guo, Z. Zhang, et al., Nano Lett. 22 (2022) 229–237.
[33] Y. Xi, J. Ge, Y. Guo, et al., ACS Nano 12 (2018) 10772–10784.
[34] C.H. Xian, Z.P. Gu, G.T. Liu, J. Wu, Chin. Chem. Lett. 31 (2020) 1612–1615.
[35] Q. Li, K. Yuan, T. Yu, et al., Biochem. Biophys. Res. Commun. 514 (2019) 618–624.